Potential Impact of Fast Flavor Oscillations on Neutrino-driven Winds and Their Nucleosynthesis

Zewei Xiong[1] , Andre Sieverding[1] , Manibrata Sen[2,3] , and Yong-Zhong Qian[1]
[1] School of Physics and Astronomy, University of Minnesota, Minneapolis, MN 55455, USA
[2] Department of Physics and Astronomy, Northwestern University, Evanston, IL 60208, USA
[3] Department of Physics, University of California, Berkeley, CA 94720, USA
Received 2020 June 19; revised 2020 July 23; accepted 2020 August 3; published 2020 September 10

Abstract

The wind driven by the intense neutrino emission from a protoneutron star (PNS) is an important site for producing nuclei heavier than the Fe group. Because of certain features in the neutrino angular distributions, the so-called fast flavor oscillations may occur very close to the PNS surface, effectively resetting the neutrino luminosities and energy spectra that drive the wind. Using the unoscillated neutrino emission characteristics from two core-collapse supernova simulations representative of relevant progenitors at the lower and higher mass end, we study the potential effects of fast flavor oscillations on neutrino-driven winds and their nucleosynthesis. We find that such oscillations can increase the total mass loss by factors up to $\sim$1.5–1.7 and lead to significantly more proton-rich conditions. The latter effect can greatly enhance the production of ^{64}Zn and the so-called light p-nuclei ^{74}Se, ^{78}Kr, and ^{84}Sr. Implications for abundances in metal-poor stars, Galactic chemical evolution in general, and isotopic anomalies in meteorites are discussed.

Unified Astronomy Thesaurus concepts: Nucleosynthesis (1131); Neutrino oscillations (1104); Supernovae (1668); Explosive nucleosynthesis (503)

1. Introduction

The collapse of the core of a massive star into a protoneutron star (PNS) results in a profuse emission of neutrinos. Simulations have shown that these neutrinos are likely a key ingredient of the explosion mechanisms for core-collapse supernovae (CCSNe) (see e.g., Bethe 1990; Wilson & Mayle 1993; Janka et al. 2012 for reviews). Further, for both the early inner ejecta (e.g., Fröhlich et al. 2006a) and the subsequent long-term neutrino-driven wind (NDW) from the PNS (e.g., Qian & Woosley 1996; Arcones et al. 2007), neutrino interactions with the material determine the conditions governing the associated nucleosynthesis, especially the electron fraction or neutron-to-proton ratio. Such neutrino-heated ejecta is potentially a major site for producing ^{64}Zn and the light p-nuclei ^{74}Se, ^{78}Kr, ^{84}Sr, and ^{92}Mo (e.g., Hoffman et al. 1996). The latter nuclei are so named because they cannot be accounted for by neutron-capture processes. Similar neutrino-driven outflows are also expected from neutron star mergers (NSMs) (e.g., Perego et al. 2014; Just et al. 2015).

Experiments with solar, atmospheric, reactor, and accelerator neutrinos have established that neutrinos oscillate among different flavors (see, e.g., Tanabashi et al. 2018 for a review). Although the effects of neutrino oscillations on CCSN explosion and nucleosynthesis have been studied for a long time (e.g., Fuller et al. 1992; Qian et al. 1993), such effects are yet to be included self-consistently in CCSN simulations. A proper treatment is difficult partly because the regular neutrino transport changes from diffusion inside the PNS to free-streaming outside it (e.g., Richers et al. 2019). In addition, because forward scattering among neutrinos causes highly nonlinear flavor evolution of the dense neutrino gas, following such evolution is effectively a new type of neutrino transport in the flavor space (see, e.g., Duan et al. 2010; Mirizzi et al. 2016 for reviews).

In this paper, we consider an interesting scenario originally suggested by Sawyer (2009), in which fast oscillations in a dense neutrino gas with certain angular distributions can cause neutrinos of different flavors with different initial emission characteristics to quickly approach flavor equilibration. Were such fast oscillations to occur near the surface of a PNS, they would reset the effective luminosities and spectra for neutrino interactions outside the PNS. In addition, were flavor equilibration to be obtained, there would be no need to consider further flavor evolution. Assuming the above features of fast flavor oscillations, we explore their impact on the NDWs and the associated nucleosynthesis. We find that such oscillations can increase the total mass loss by factors up to $\sim$1.5–1.7 and lead to significantly more proton-rich conditions. The latter effect can greatly enhance the production of ^{64}Zn and the light p-nuclei ^{74}Se, ^{78}Kr, and ^{84}Sr.

This paper is organized as follows. We describe our NDW models with fast flavor oscillations in Section 2. We present the effects of such oscillations on NDWs in Section 3 and those on nucleosynthesis in Section 4. Implications for abundances in metal-poor stars, Galactic chemical evolution in general, and isotopic anomalies in meteorites are discussed in Section 5. Further discussion and conclusions are given in Section 6.

2. Modeling NDWs with Fast Flavor Oscillations

Fast neutrino flavor oscillations have been examined by many studies (e.g., Capozzi et al. 2017, 2019; Izaguirre et al. 2017; Abbar & Duan 2018; Dasgupta & Sen 2018; Abbar & Volpe 2019; Delfan Azari et al. 2019, 2020; Martin et al. 2019; Nagakura et al. 2019; Yi et al. 2019; Abbar et al. 2020; Glas et al. 2020). Wu & Tamborra (2017) found that conditions for such oscillations appear to be ubiquitous in NSMs, which has important implications for nucleosynthesis and future kilonova observations if flavor equilibration is obtained (Wu et al. 2017). Whether conditions for fast flavor oscillations are prevalent in

CCSNe depends sensitively on detailed neutrino transport calculations. We do not take up this important issue here. Instead, we assume that such oscillations occur during the long-term cooling of the PNS and explore their effects on the NDW and the associated nucleosynthesis.

We consider three different assumptions for neutrino oscillations. We take the neutrino luminosities and energy spectra from representative CCSN simulations and assume no flavor oscillations for our baseline models. As a limiting case, we assume that fast flavor oscillations result in complete flavor equilibration for the neutrino fluxes driving the winds. Specifically, the oscillated spectral fluxes are

$$F_{\nu_e}^{\rm osci} = F_{\nu_x}^{\rm osci} = \frac{F_{\nu_e}^0 + 2F_{\nu_x}^0}{3}, \qquad (1a)$$

$$F_{\bar{\nu}_e}^{\rm osci} = F_{\bar{\nu}_x}^{\rm osci} = \frac{F_{\bar{\nu}_e}^0 + 2F_{\bar{\nu}_x}^0}{3}, \qquad (1b)$$

where $F_{\nu_e}^0$, $F_{\bar{\nu}_e}^0$, and $F_{\nu_x}^0 = F_{\bar{\nu}_x}^0$ are the unoscillated spectral fluxes and x stands for μ or τ. Note, however, that the above expressions represent an approximate limit because flavor equilibration is subject to conservation of flavor lepton number (Dasgupta & Sen 2018; Abbar & Volpe 2019). As an intermediate case, we take the results from Dasgupta et al. (2017), who modeled fast flavor oscillations by introducing small artificial anisotropies in the neutrino angular distributions from a spherically symmetric CCSN simulation. In this case, the oscillated spectral fluxes are

$$F_{\nu_e}^{\rm osci} = P_{ee}F_{\nu_e}^0 + (1 - P_{ee})F_{\nu_x}^0, \qquad (2a)$$

$$F_{\bar{\nu}_e}^{\rm osci} = P_{\bar{e}\bar{e}}F_{\bar{\nu}_e}^0 + (1 - P_{\bar{e}\bar{e}})F_{\bar{\nu}_x}^0, \qquad (2b)$$

$$F_{\nu_x}^{\rm osci} = \frac{1 - P_{ee}}{2}F_{\nu_e}^0 + \frac{1 + P_{ee}}{2}F_{\nu_x}^0, \qquad (2c)$$

$$F_{\bar{\nu}_x}^{\rm osci} = \frac{1 - P_{\bar{e}\bar{e}}}{2}F_{\bar{\nu}_e}^0 + \frac{1 + P_{\bar{e}\bar{e}}}{2}F_{\bar{\nu}_x}^0, \qquad (2d)$$

where $P_{ee} = 0.68$ and $P_{\bar{e}\bar{e}} = 0.55$. Note that these values are not based on self-consistent CCSN simulations but represent plausible results intermediate between the cases of no flavor oscillations and complete flavor equilibration. There is no need to consider further neutrino oscillations for the case of complete flavor equilibration. We do not consider other types of oscillations for the case of intermediate flavor conversion, either.

For the unoscillated spectral fluxes, we take the neutrino luminosities and average energies as functions of time from two CCSN simulations. The normalized spectrum is taken to be Fermi–Dirac with zero chemical potential and is characterized by a temperature for each neutrino species. Neutrino emission is not expected to vary drastically among progenitors whose CCSNe would result in long-term NDWs. Nevertheless, there are some trends and characteristics that distinguish the emission for relevant progenitors (Janka et al. 2012). In particular, more massive progenitors are expected to be associated with an extended phase of accretion-driven neutrino emission, whereas low-mass ones can explode more promptly and thus exhibit a faster decline of the neutrino luminosities. We adopt the results from two representative state-of-the-art CCSN simulations in spherical symmetry with detailed long-term neutrino transport. One simulation (Hüdepohl et al. 2010) was based on the
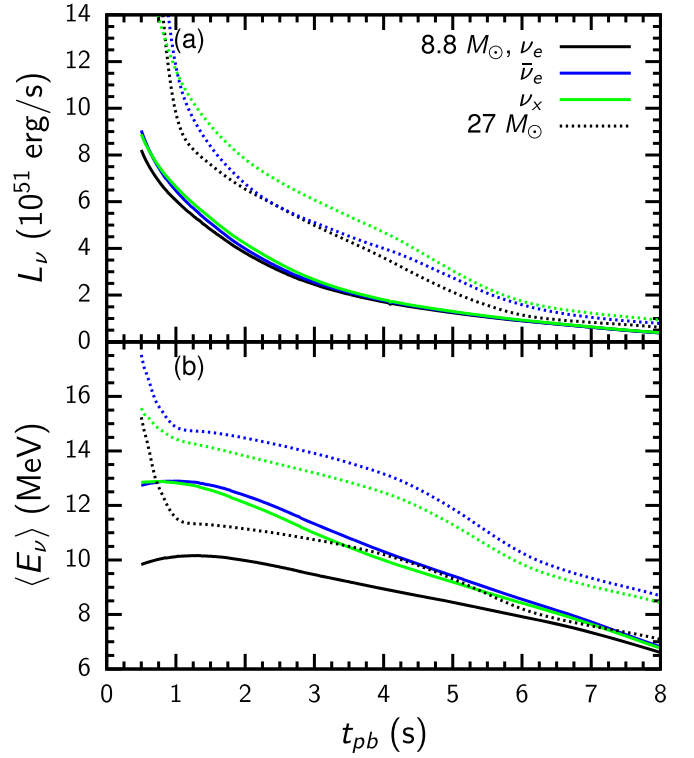

Figure 1. Time evolution of (a) luminosities L_ν and (b) average energies $\langle E_\nu \rangle$ for ν_e (black), $\bar{\nu}_e$ (blue), and ν_x (green) for models e8.8 (solid curves) and s27 (dashed curves).

8.8 $M_\odot$ progenitor model of Nomoto (1984). We will refer to the corresponding neutrino emission model as model e8.8. The other model, reported in Mirizzi et al. (2016) and referred to as model s27, is from a simulation based on a 27 $M_\odot$ progenitor model of Woosley et al. (2002). Note that explosion was triggered artificially for model s27. The time evolution of neutrino luminosities and average energies for models e8.8 and s27 is shown in Figure 1. These results are considered as representative of neutrino emission for relevant progenitors at the lower and higher mass end.

All neutrinos are assumed to be emitted from a sharp neutrino sphere whose radius R_ν evolves with time post core bounce $t_{\rm pb}$ as

$$R_\nu = \left[12 + 8.5\left(\frac{1\,{\rm s}}{t_{\rm pb}}\right)^{0.7}\right]{\rm km}. \qquad (3)$$

The above result is fitted to model e8.8 and assumed to apply to model s27 as well. In view of this assumption, we also take the same PNS mass $M_{\rm PNS} = 1.282\,M_\odot$ for both models. While the above assumptions would cause some uncertainties in the NDW properties for model s27, they would not significantly affect the comparison between the corresponding cases with and without fast flavor oscillations. As we will show below, the dominant effect of such oscillations is to increase the electron fraction. This effect depends on the unoscillated neutrino luminosities and spectra, which are taken directly from the CCSN models without approximation.

Because the timescales for evolution of R_ν and neutrino emission are sufficiently long, we model the NDW as a steady-state outflow from the neutrino sphere. For a specific $t_{\rm pb}$, we solve the velocity v, density ρ, temperature T, and electron

fraction Y_e of the NDW as functions of radius r from the following equations:

$$\dot{M} = 4\pi r^2 \rho v, \tag{4a}$$

$$v\frac{dv}{dr} = -\frac{1}{\rho}\frac{dP}{dr} - \frac{GM_{\mathrm{PNS}}}{r^2}, \tag{4b}$$

$$\frac{d\epsilon}{dr} = \frac{P}{\rho^2}\frac{d\rho}{dr} + \frac{\dot{q}}{v}, \tag{4c}$$

$$\frac{dY_e}{dr} = \frac{1}{v}[(\lambda_{\nu_e n} + \lambda_{e^+ n})Y_n - (\lambda_{\bar{\nu}_e p} + \lambda_{e^- p})Y_p], \tag{4d}$$

where $\dot{M}$ is the mass-loss rate; P is the pressure; G is the gravitational constant; ϵ is the internal energy per unit mass; $\dot{q}$ is the rate of net energy gain per unit mass; Y_n (Y_p) is the number of free neutrons (protons) per baryon, i.e., the number fraction of free neutrons (protons); and $\lambda_{\nu_e n}$ ($\lambda_{e^- p}$) and $\lambda_{\bar{\nu}_e p}$ ($\lambda_{e^+ n}$) are the rates per target nucleon for the ν_e and $\bar{\nu}_e$ absorption reactions (inverse reactions), respectively. Because neutrino heating mainly occurs before any significant synthesis of heavy elements, the nuclear composition is taken to be free nucleons in nuclear statistical equilibrium (NSE) with α-particles when the above equations are solved. The details of $P, \epsilon, \dot{q}$, and the rates for determining Y_e are given in Xiong et al. (2019). For each of the three cases of neutrino oscillations, the corresponding neutrino rates for heating the wind and determining Y_e are used.

At each t_{pb}, the inner boundary conditions of the steady-state solution are specified by $\dot{q} = 0$, $dY_e/dr = 0$, and $T = T_{\nu_e}$ at $r = R_\nu$, where T_{ν_e} is the temperature of the initial ν_e spectrum. These conditions correspond to approximate equilibrium between matter and neutrinos at the neutrino sphere. In principle, the mass-loss rate $\dot{M}$ should be obtained as an eigenvalue to satisfy the outer boundary condition imposed by the earlier CCSN ejecta on the NDW. Because the outer boundary, or the wind-termination point, at $r = r_{\mathrm{wt}}$ is outside the region of efficient neutrino heating, the actual solution is well approximated by the transonic solution for $r \lesssim r_{\mathrm{wt}}$ (Qian & Woosley 1996). As the outer boundary evolves with t_{pb} and varies with CCSN progenitors, for simplicity, we adopt the transonic solution up to $r_{\mathrm{wt}} = 1000$ km for both models e8.8 and s27 (e.g., Arcones et al. 2007; Arcones & Janka 2011), but also consider $r_{\mathrm{wt}} = 500$ km for model s27 to cover the range of NDW solutions (e.g., Wanajo et al. 2011a). At $r_{\mathrm{wt}} = 1000$ km, the temperature is typically below 1 GK, which corresponds to NDW interaction with the CCSN ejecta without generating a strong shock. At $r_{\mathrm{wt}} = 500$ km, the temperature can be up to 3 GK, which is still appropriate for postshock material.

The steady-state profiles are calculated for many values of t_{pb} to give v, T, ρ, and Y_e on a 2D grid of r and t. The trajectory of a tracer in the NDW is calculated from $r(t) = r(t_0) + \int_{t_0}^{t} v(r(t'), t')dt'$ and the associated T, ρ, and Y_e are obtained by interpolating the corresponding profiles on the 2D grid. As the steady-state solutions have approximately reached the asymptotic velocity at $r_{\mathrm{wt}} = 1000$ km, we assume $v(t) = v_{\mathrm{wt}}$ and

$$r(t) = r_{\mathrm{wt}} + v_{\mathrm{wt}}(t - t_{\mathrm{wt}}) \tag{5}$$

for $r > 1000$ km. Here and below, the subscript "wt" denotes quantities at $r = r_{\mathrm{wt}}$. For $r_{\mathrm{wt}} = 500$ km, the steady-state NDWs should be slowed down before reaching the asymptotic

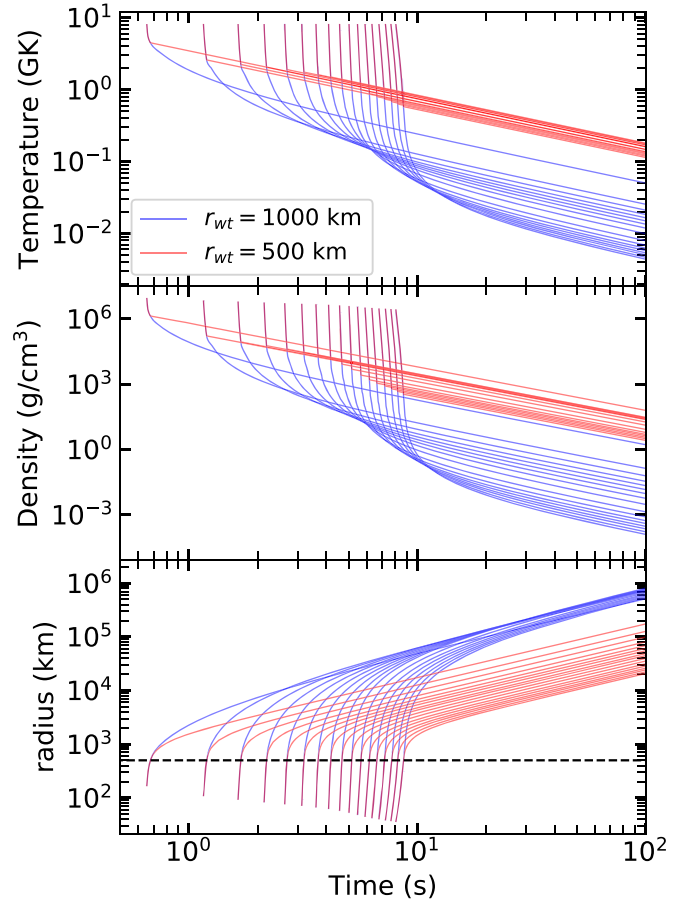**Figure 2.** Evolution of temperature (top panel), density (middle panel), and radius (bottom panel) for example tracers in model s27 with $r_{\mathrm{wt}} = 1000$ (blue curves) and 500 km (red curves) in the case of no flavor oscillations. The horizontal dashed line in the bottom panel indicates $r_{\mathrm{wt}} = 500$ km.

velocity. So we assume

$$r(t) = r_{\mathrm{wt}}\left[1 - \frac{v_{\mathrm{wt}}t_{\mathrm{wt}}}{r_{\mathrm{wt}}} + \frac{v_{\mathrm{wt}}t_{\mathrm{wt}}}{r_{\mathrm{wt}}}\left(\frac{t}{t_{\mathrm{wt}}}\right)^3\right]^{1/3} \tag{6}$$

for $r > r_{\mathrm{wt}}$ in this case, where $v(t) = dr/dt$ has an asymptotic value of $v_{\mathrm{wt}}[r_{\mathrm{wt}}/(v_{\mathrm{wt}}t_{\mathrm{wt}})]^{2/3} < v_{\mathrm{wt}}$ (Wanajo et al. 2011a). For both $r_{\mathrm{wt}} = 1000$ and 500 km, we assume $r^2 \rho v = r_{\mathrm{wt}}^2 \rho_{\mathrm{wt}} v_{\mathrm{wt}}$ and $T^3/\rho = T_{\mathrm{wt}}^3/\rho_{\mathrm{wt}}$ to extrapolate $\rho(t)$ and $T(t)$ for $r > r_{\mathrm{wt}}$ (e.g., Ning et al. 2007; Wanajo et al. 2011a). In this approach, we neglect any entropy jump due to the possible formation of a reverse shock at r_{wt} (Arcones et al. 2007). The evolution of Y_e is followed along with nucleosynthesis for the tracer and will be discussed in Section 4.

Figure 2 shows $T(t)$, $\rho(t)$, and $r(t)$ for example tracers in model s27 with $r_{\mathrm{wt}} = 1000$ and 500 km in the case of no flavor oscillations. It can be seen that for $r_{\mathrm{wt}} = 500$ km, the temperature and density stay at relatively high values for longer time. The corresponding effects on nucleosynthesis will be discussed in Section 4.

3. Effects of Fast Flavor Oscillations on NDWs
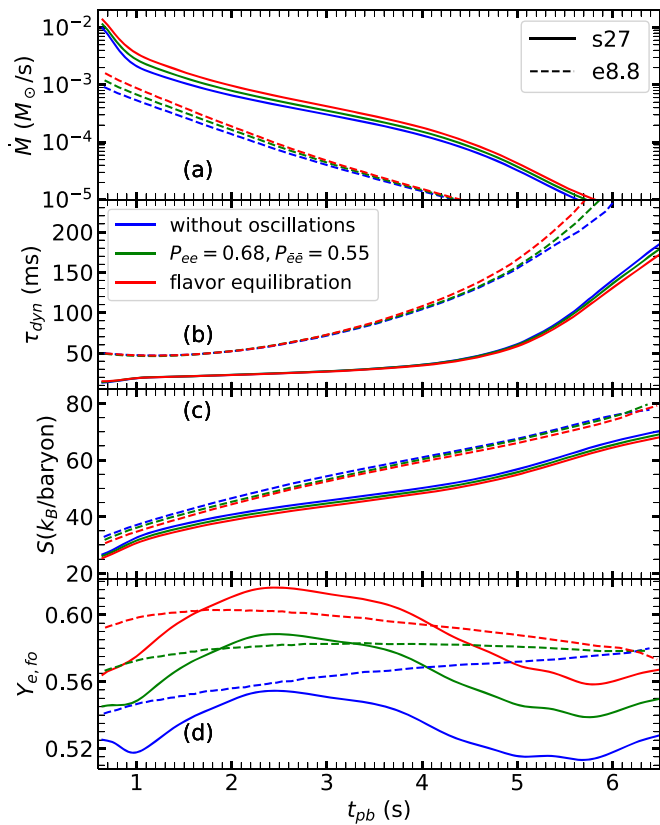
The main heating processes for driving the wind are

$$\nu_e + n \rightarrow p + e^-, \tag{7a}$$

Figure 3. Evolution of the mass-loss rate $\dot{M}$, dynamical timescale τ_{dyn} and entropy S taken at $T = 0.5$ MeV, and freeze-out electron fraction $Y_{e,\mathrm{fo}}$ taken at $T = 3$ GK. Each panel shows the results for models e8.8 (dashed curves) and s27 (solid curves), both with $r_{\mathrm{wt}} = 1000$ km, in the cases of no flavor oscillations (blue curves), intermediate flavor conversion (green curves), and complete flavor equilibrium (red curves).

$$\bar{\nu}_e + p \rightarrow n + e^+, \tag{7b}$$
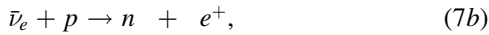
which also set the important parameter Y_e for nucleosynthesis. Figure 1 shows that for nearly the entire duration of the NDW, ν_x ($\bar{\nu}_x$) has higher luminosity and average energy than ν_e ($\bar{\nu}_e$) for model s27. In comparison, for model e8.8, the luminosities are close for all neutrino species; $\bar{\nu}_x$ and $\bar{\nu}_e$ also have very similar average energy, but ν_x still has higher average energy than ν_e. As fast flavor oscillations convert ν_x ($\bar{\nu}_x$) into ν_e ($\bar{\nu}_e$), heating by the reactions in Equation (7) is enhanced, which produces a higher mass-loss rate $\dot{M}$ (see Figure 3) and, hence, a higher net mass loss in the NDW. Indeed, as shown in Table 1, the net mass loss increases by a factor of ~1.7 and 1.5 (1.3 and 1.2) for models e8.8 and s27, respectively, in the case of complete flavor equilibrium (intermediate flavor conversion). The mass-loss rate for model s27 is higher than that for model e8.8 because of the higher neutrino luminosities and average energies for the former.

As we will discuss in Section 4, production of heavy nuclei in the NDW depends on the ratio of protons to seed nuclei (heavier than ^{4}He), which is sensitive to the dynamical timescale for the earlier expansion of a tracer. Following Qian & Woosley (1996), we define this quantity as

$$\tau_{\mathrm{dyn}} = (r/v)_{T=0.5\,\mathrm{MeV}}, \tag{8}$$

which is calculated when the temperature of a tracer drops to $T = 0.5$ MeV. Higher neutrino luminosities and average

energies drive faster winds. So τ_{dyn} for model e8.8 is longer than that for model s27 for the same $r_{\mathrm{wt}} = 1000$ km, and τ_{dyn} for both models increases with time (see Figure 3). For $t_{\mathrm{pb}} \lesssim 5$ s, the effect of fast flavor oscillations on τ_{dyn} is $\lesssim 10\%$ even for complete flavor equilibration. Only at late times when there is little mass ejected in the NDW (see Figure 3) does this effect increase to up to ~20%. The entropy is another important quantity for setting the proton-to-seed ratio. The value (in units of Boltzmann constant k_{B} per baryon) taken at $T = 0.5$ MeV is also shown in Figure 3. The effect of fast flavor oscillations on the entropy is only $\lesssim 7\%$ for complete flavor equilibration over the duration of the NDW in our calculations.

Yet another important quantity for nucleosynthesis in the NDW is the freeze-out electron fraction $Y_{e,\mathrm{fo}}$ (taken at $T = 3$ GK), which is determined by the competition between the reactions in Equation (7). Specifically, $Y_{e,\mathrm{fo}} > 0.5$ when $\langle E_{\bar{\nu}_e} \rangle - \langle E_{\nu_e} \rangle$ lies below some multiple of the neutron-to-proton mass difference (Qian & Woosley 1996). Without flavor oscillations, $Y_{e,\mathrm{fo}} > 0.5$ and the NDW is proton-rich for both models e8.8 and s27. As fast flavor oscillations increase the effective luminosity and average energy of ν_e more than those of $\bar{\nu}_e$, they make the NDW more proton-rich (see Figure 3). Because the difference in luminosity and average energy between ν_x and ν_e for model s27 is larger than that for model e8.8, the increase of $Y_{e,\mathrm{fo}}$ due to fast flavor oscillations for the former is larger than that for the latter. In addition, for model e8.8, the luminosities and average energies of all neutrino species become closer with time, so the effect of fast flavor oscillations on $Y_{e,\mathrm{fo}}$ is greatly reduced at late times. The maximum values of $Y_{e,\mathrm{fo}}$ for different models of the NDW are compared in Table 1.

Because the mass-loss rate, τ_{dyn}, entropy, and $Y_{e,\mathrm{fo}}$ are set by neutrino reactions well inside the wind-termination point, the effects of fast flavor oscillations on the above quantities are the same for model s27 with either $r_{\mathrm{wt}} = 1000$ or 500 km. The main differences between these two cases are in the evolution of temperature and density for $r > 500$ km (see Figure 2). The much slower expansion at later times for the NDW with $r_{\mathrm{wt}} = 500$ km amplifies the effects of $Y_{e,\mathrm{fo}}$ on nucleosynthesis by allowing more neutron production and subsequent proton capture (see Section 4).

4. Effects of Fast Flavor Oscillations on Nucleosynthesis

Proton-rich NDWs (Arcones & Thielemann 2013; Martínez-Pinedo et al. 2014) are considered an important site for the νp process (Fröhlich et al. 2006b; Fischer et al. 2012; Bliss et al. 2018), which can produce the light p-nuclei under suitable conditions, thereby affecting their chemical evolution (Travaglio et al. 2018). In a hot proton-rich environment, competition between (p, γ) and (γ, p) reactions results in waiting-point nuclei that dominate the abundance in the associated isotopic chain, and their β decays control the progress to heavier nuclei. In the νp process, however, slow β decays are overcome by (n, p) reactions, for which neutrons are provided by $\bar{\nu}_e$ absorption on protons (Fröhlich et al. 2006b). For efficient production of heavy nuclei, neutron production should take place at ~1–3 GK so that the temperature is sufficiently high to overcome the increasingly high Coulomb barrier for further proton capture, but low enough to avoid strong photodissociation.

Table 1
Effects of Fast Flavor Oscillations on the NDW (see also Figure 3) and the νp Process

Models	Oscillations	Mass Loss ($10^{-3}M_\odot$)	$Y_{e,\mathrm{fo}}^{\max}$	$\Delta_{n,\max}$
e8.8, $r_{\mathrm{wt}} = 1000$ km	without oscillations	0.79	0.64	3.12
e8.8, $r_{\mathrm{wt}} = 1000$ km	$P_{ee} = 0.68$, $P_{\bar{e}\bar{e}} = 0.55$	1.06	0.65	3.70
e8.8, $r_{\mathrm{wt}} = 1000$ km	flavor equilibration	1.33	0.66	3.91
s27, $r_{\mathrm{wt}} = 1000$ km	without oscillations	3.64	0.55	1.10
s27, $r_{\mathrm{wt}} = 1000$ km	$P_{ee} = 0.68$, $P_{\bar{e}\bar{e}} = 0.55$	4.43	0.59	2.31
s27, $r_{\mathrm{wt}} = 1000$ km	flavor equilibration	5.48	0.61	3.67
s27, $r_{\mathrm{wt}} = 500$ km	without oscillations	3.64	0.55	2.48
s27, $r_{\mathrm{wt}} = 500$ km	$P_{ee} = 0.68$, $P_{\bar{e}\bar{e}} = 0.55$	4.43	0.59	5.34
s27, $r_{\mathrm{wt}} = 500$ km	flavor equilibration	5.48	0.61	8.94

4.1. Effectiveness of the vp Process

The effectiveness of the νp process is mainly determined by the proton-to-seed ratio Y_p/Y_h and the net neutron abundance provided by $\bar{\nu}_e$ absorption on protons. The ratio Y_p/Y_h, where Y_h is the number fraction of nuclei heavier than ^{4}He, specifies the availability of protons for neutron production and further proton capture subsequent to (n, p) reactions. Following Pruet et al. (2006), we define

$$\Delta_n = \left(\frac{Y_p}{Y_h}\right)_{T=3\,\mathrm{GK}} \times \int_{T<3\,\mathrm{GK}} \lambda_{\bar{\nu}_e p}\, dt, \qquad (9)$$

which measures the overall effectiveness of the νp process. For a high Δ_n, the NDW should have high entropy and fast expansion down to $T \sim 3$ GK to ensure a high $(Y_p/Y_h)_{T=3\,\mathrm{GK}}$, as well as slow expansion at lower temperatures to ensure sufficient neutrino exposure for neutron production. Slow expansion at $T \sim 1$–3 GK also facilitates further proton capture to make heavier nuclei.

Figure 4 shows that fast flavor oscillations can increase $(Y_p/Y_h)_{T=3\,\mathrm{GK}}$ by up to a factor ~ 3 (~ 2) for model s27 (e8.8) with $r_{\mathrm{wt}} = 1000$ km. Qualitatively, these effects are similar to those on $Y_{e,\mathrm{fo}}$ shown in Figure 3. With the additional increase of $\lambda_{\bar{\nu}_e p}$, fast flavor oscillations also increase Δ_n (see Figure 5). While these effects are quite noticeable, Δ_n does not exceed 4 even with complete flavor equilibration for models e8.8 and s27 with $r_{\mathrm{wt}} = 1000$ km (see Table 1). In contrast, for model s27 with $r_{\mathrm{wt}} = 500$ km, while $(Y_p/Y_h)_{T=3\,\mathrm{GK}}$ is the same as for $r_{\mathrm{wt}} = 1000$ km, Δ_n is increased to up to ~ 9 with complete flavor equilibration because the duration corresponding to $T \sim 1$–3 GK is much longer (see Figure 2). The light p-nucleus ^{84}Sr is the heaviest isotope noticeably produced in our models. Its mass fraction produced by each tracer is shown in Figure 5 and clearly follows the trend of Δ_n.

4.2. Results on Nucleosynthesis

We calculate the nucleosynthesis for each tracer with the reaction network used in Sieverding et al. (2018). Thermonuclear reaction rates are taken from the ReaclibV2.2 library (Cyburt et al. 2010), and β-decay rates are taken from the NUBASE compilation of experimental values (Audi et al. 2017) when available and from Möller et al. (2003) otherwise. The only neutrino reactions included are those in Equation (7), with the same rates used for modeling the NDW. Beyond the
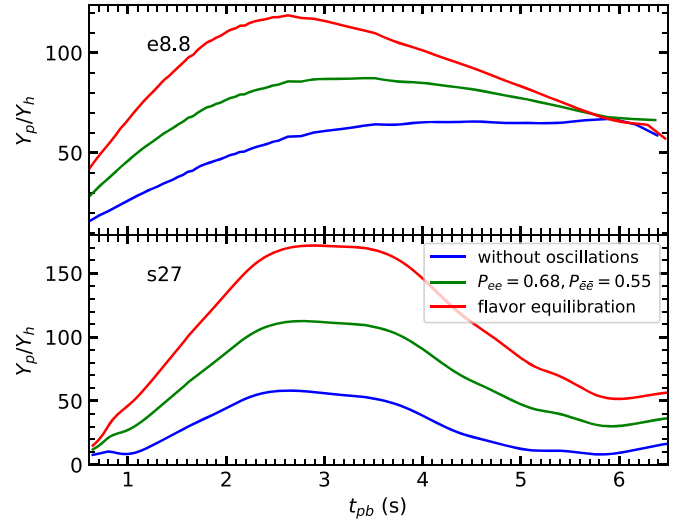

Figure 4. Proton-to-seed ratio Y_p/Y_h at $T = 3$ GK for models e8.8 and s27 with $r_{\mathrm{wt}} = 1000$ km in the cases of no flavor oscillations (blue curves), intermediate flavor conversion (green curves), and complete flavor equilibration (red curves).

wind-termination point, we use, for example,

$$\lambda_{\bar{\nu}_e p}(t) = \lambda_{\bar{\nu}_e p}(t_{\mathrm{wt}}) \left[\frac{r_{\mathrm{wt}}}{r(t)}\right]^2 \exp\left(-\frac{t - t_{\mathrm{wt}}}{\tau_\nu}\right), \qquad (10)$$

where the exponential factor with $\tau_\nu = 3$ s approximately accounts for the decrease of neutrino luminosities with time. Using the neutrino rates, which include corrections for weak magnetism and nucleon recoil (see Xiong et al. 2019 for details), we follow the evolution of Y_e for a tracer, taking into account the change of the detailed nuclear composition. We find very good agreement with the Y_e calculated by the NDW models during the time when dynamic and thermodynamic properties of the NDW are being determined. Apart from this check of consistency, including the neutrino reactions, especially $\bar{\nu}_e$ absorption on protons, is required to follow the evolution of the neutron abundance for the νp process.

For convenience, we label a tracer with the time t_{wt} at which it reaches the wind-termination radius r_{wt}. Our reaction network calculations give the final mass fraction $X(Z, A, t_{\mathrm{wt}})$ for a nucleus with charge number Z and mass number A for the
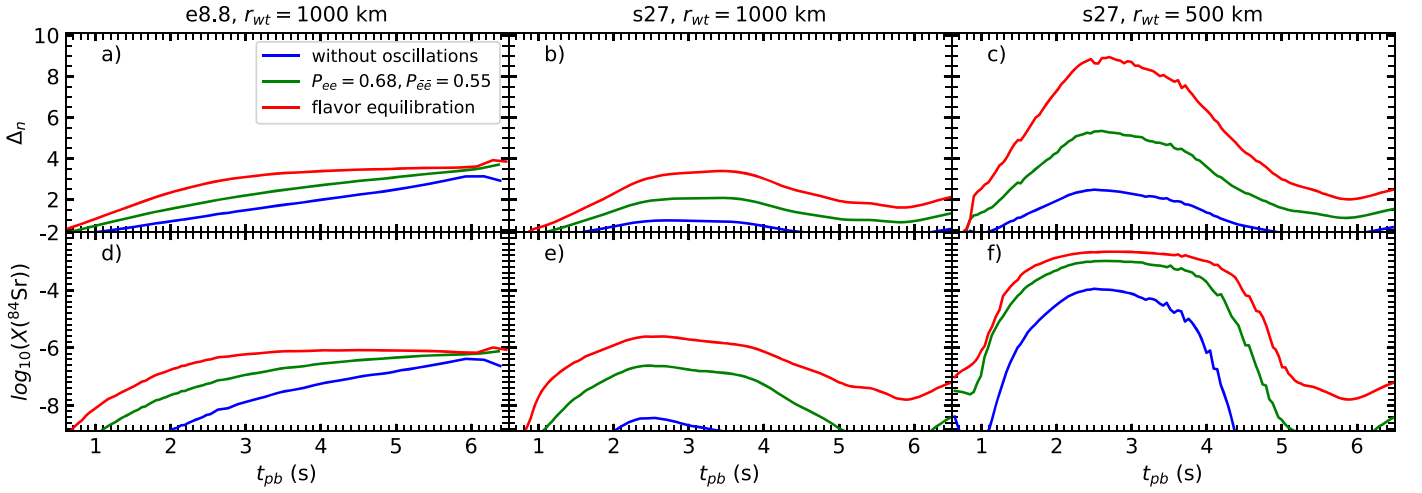
Figure 5. Comparison of Δ_n and ^{84}Sr mass fraction for different NDW models in the cases of no flavor oscillations (blue curves), intermediate flavor conversion (green curves), and complete flavor equilibrium (red curves).

tracer. Each tracer is also associated with a mass-loss rate $\dot{M}(t_{wt})$. So the integrated yield of a nucleus is

$$y(Z, A) = \int X(Z, A, t_{wt})\dot{M}(t_{wt}) \, dt_{wt}, \qquad (11)$$

which is evaluated with 72 and 184 tracers for models e8.8 and s27, respectively.

The integrated yields are shown in Figure 6 for different NDW models in the cases of no flavor oscillations, intermediate flavor conversion, and complete flavor equilibrium. Yields of ^{64}Zn and the light p-nuclei ^{74}Se, ^{78}Kr, ^{84}Sr, ^{92}Mo, and ^{96}Ru are also given in Table 2. The integrated yields contain large contributions from those NDWs whose conditions are not favorable to the νp process but only give rise to an α-rich freeze-out. The resulting yield patterns are very similar for models e8.8 and s27 with $r_{wt} = 1000$ km in all the cases, with the mass fraction of ^{4}He being the largest followed by that of ^{56}Fe. There are also peaks at ^{60}Ni with a closed shell of $Z = 28$ protons and at ^{64}Zn resulting from the decay of ^{64}Ge. Note that ^{64}Ge is the first important waiting-point nucleus for proton-rich nucleosynthesis (Pruet et al. 2005). Its slow β-decay, which effectively blocks production of heavier nuclei, is overcome by the (n, p) reaction following neutron production by $\bar{\nu}_e$ absorption on protons in the νp process.

For model e8.8, the yield exceeds $\sim 10^{-7} M_\odot$ for nuclei between ^{56}Fe and $A = 68$ but drops steeply for heavier nuclei due to the inefficiency of the νp process. Fast flavor oscillations increase the yields of nuclei heavier than ^{56}Fe. In particular, the yield of ^{64}Zn is increased by a factor of ~ 4 with complete flavor equilibration (see Table 2). Such oscillations, however, do not extend significantly the range of heavy nuclei with yields of $\gtrsim 10^{-7} M_\odot$. Specifically, the yields of the light p-nuclei are still rather low, although they are dramatically increased with fast flavor oscillations. For model s27 with the same $r_{wt} = 1000$ km, the mass-loss rates are higher than those for model e8.8 in general (see Figure 3), and the highest Δ_n values are also reached when the mass-loss rates are relatively high (see Figure 5). Consequently, the yields of nuclei heavier than ^{56}Fe are higher than those for model e8.8, and the effects of fast flavor oscillations are also noticeably stronger, extending nuclei with yields of $\gtrsim 10^{-7} M_\odot$ up to the light p-nucleus ^{74}Se (see Figure 6 and Table 2).
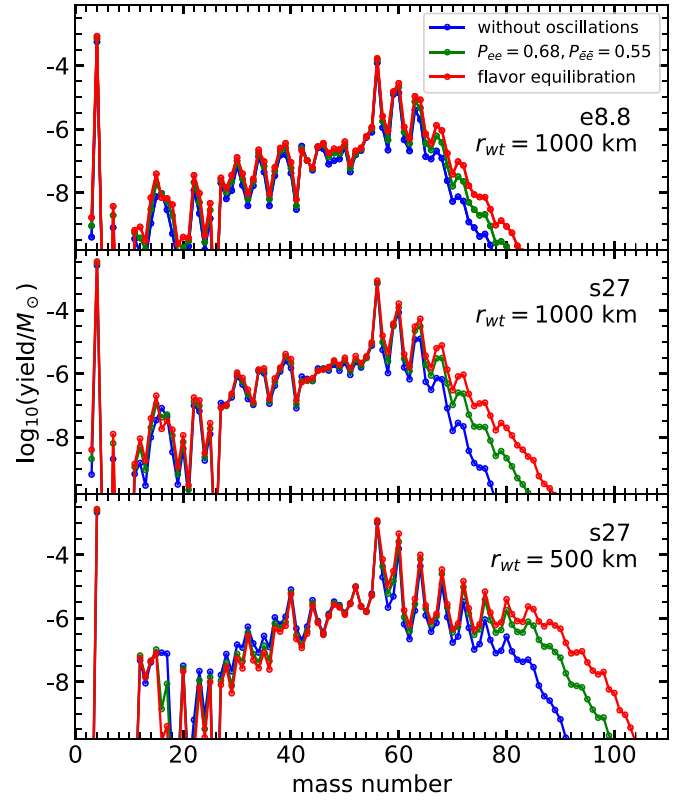

Figure 6. Comparison of nucleosynthesis yields for different NDW models in the cases of no flavor oscillations (blue curves), intermediate flavor conversion (green curves), and complete flavor equilibrium (red curves).

For model s27 with $r_{wt} = 500$ km, the yield exceeds $\sim 10^{-7} M_\odot$ for heavy nuclei up to $A = 80$ even without flavor oscillations, reflecting the corresponding relatively large Δ_n values (see Figure 5). With complete flavor equilibration, the range of nuclei with yields of $\gtrsim 10^{-7} M_\odot$ is extended up to ^{90}Zr and ^{91}Zr, and even the light p-nuclei ^{92}Mo and ^{96}Ru are produced with substantial yields of 7.83×10^{-8} and $2.24 \times 10^{-8} M_\odot$, respectively (see Table 2). Fast flavor oscillations also reduce the yields of nuclei with $A < 60$ while increasing those of heavier ones, clearly indicating the

Table 2
Yields (in $M_\odot$) for ^{64}Zn and Selected Light p-Nuclei for Different NDW Models [$X(Y)$ Denotes $X \times 10^Y$]

Model	Oscillations	^{64}Zn	^{74}Se	^{78}Kr	^{84}Sr	^{92}Mo	^{96}Ru
e8.8, $r_{\rm wt} = 1000$ km	without oscillations	2.00(−6)	7.88(−10)	5.90(−11)	3.55(−12)	8.77(−15)	3.53(−16)
e8.8, $r_{\rm wt} = 1000$ km	$P_{ee} = 0.68, P_{\bar{e}\bar{e}} = 0.55$	4.62(−6)	2.90(−9)	2.58(−10)	1.91(−11)	6.05(−14)	2.64(−15)
e8.8, $r_{\rm wt} = 1000$ km	flavor equilibration	8.33(−6)	8.68(−9)	9.39(−10)	9.49(−11)	4.64(−13)	2.42(−14)
s27, $r_{\rm wt} = 1000$ km	without oscillations	1.25(−5)	1.53(−9)	9.59(−11)	1.77(−12)	7.99(−16)	1.46(−17)
s27, $r_{\rm wt} = 1000$ km	$P_{ee} = 0.68, P_{\bar{e}\bar{e}} = 0.55$	3.08(−5)	2.16(−8)	2.56(−9)	1.74(−10)	4.42(−13)	1.22(−14)
s27, $r_{\rm wt} = 1000$ km	flavor equilibration	5.33(−5)	9.57(−8)	1.64(−8)	2.44(−9)	1.84(−11)	9.27(−13)
s27, $r_{\rm wt} = 500$ km	without oscillations	4.34(−5)	1.03(−7)	7.98(−8)	4.95(−8)	6.70(−11)	3.54(−12)
s27, $r_{\rm wt} = 500$ km	$P_{ee} = 0.68, P_{\bar{e}\bar{e}} = 0.55$	7.27(−5)	3.00(−7)	3.51(−7)	7.76(−7)	8.16(−9)	1.33(−9)
s27, $r_{\rm wt} = 500$ km	flavor equilibration	9.92(−5)	4.34(−7)	6.14(−7)	2.34(−6)	7.83(−8)	2.24(−8)

enhancement of the νp process by such oscillations (see Figure 6).

5. Implications

In this section, we discuss the implications of our NDW models with fast flavor oscillations for abundances in metal-poor stars, Galactic chemical evolution in general, and isotopic anomalies in meteorites. Our main goal is to propose potential connections to the above broad topics based on our results. Using observations and measurements as guidance, we will try to be quantitative, but will necessarily invoke speculation because there are many currently unresolved issues, such as the mixing and ejection of CCSN nucleosynthesis products. We caution that our discussion is meant more to stimulate further work than to reach firm conclusions.

5.1. Abundances in Metal-poor Stars

Metal-poor stars were formed out of the interstellar medium (ISM) at very early times, and their surface abundances reflect chemical enrichment by only a small number of nucleosynthetic events prior to their formation (e.g., Frebel 2018). Consequently, the abundances in such a star may show some features of the nucleosynthesis of a CCSN at low metallicities. Because ^{64}Zn is a major product of NDWs, which most likely remains true of low-metallicity CCSNe, we estimate [Zn/Fe] = log(Zn/Fe) − log(Zn/Fe)$_\odot$ using the Zn yields from our NDW models along with the Fe yields from the associated CCSNe, and compare the results with the data on metal-poor stars. We include all the isotopes of the same element in the results presented below.

For the CCSN associated with model e8.8, explosive nucleosynthesis produces $\sim$0.002–0.004 $M_\odot$ of Fe (Wanajo et al. 2009), which greatly exceeds the amount [$\sim$(1–2) × $10^{-4}\,M_\odot$] produced in the NDWs with or without flavor oscillations. Assuming that the Zn and Fe yields apply at low metallicities, we expect [Zn/Fe] $\sim$−0.5 to −0.2, −0.1 to 0.2, and 0.2–0.5 from our NDW models without flavor oscillations, with intermediate flavor conversion, and with complete flavor equilibration, respectively. The above results on [Zn/Fe] would correspond to [Fe/H] $\sim$−3.7 to −2.4, with the CCSN enriching $\sim$10^3–10$^4\,M_\odot$ of ISM. Observations (Cayrel et al. 2004) show that stars with [Fe/H] $\sim$−4.4 to −2.5 have [Zn/Fe] $\sim$0.1–0.7. So it appears that NDWs from CCSNe with progenitors and neutrino emission similar to those of model e8.8 can account for some of the data on [Zn/Fe] for metal-poor stars only when fast flavor oscillations are included.

For low-metallicity CCSNe with progenitors and neutrino emission similar to those of model s27, we expect a much wider range of Fe yields due to the great uncertainties in the explosion mechanism and the role of mixing and fallback. Assuming the Zn yields from our NDW models, we find that a nominal Fe yield of $\sim$0.1 $M_\odot$ would give low values of [Zn/Fe] $< −0.1$ for model s27 with $r_{\rm wt} = 1000$, km or 500 km regardless of flavor oscillations. It is also plausible, however, that the low-metallicity CCSNe of concern undergo weak explosion, in which most of the He-core falls back onto the PNS (most likely resulting in the formation of a black hole) and only a small fraction of the inner nucleosynthesis products are mixed into the ejecta. The transitional existence of the PNS would still allow a NDW to form and a fraction of this material to be mixed into the ejecta. We explore such a scenario below to explain the high values of both [Zn/Fe] and [Sr/Fe] in the metal-poor star HE 1327–2326 (Ezzeddine et al. 2019).

Because of the uncertainties in the Fe yield and the ejected fraction, we first seek to explain [Sr/Zn] $\sim$0 $\pm$ 0.3 for HE 1327–2326 (Ezzeddine et al. 2019). Because our model s27 with $r_{\rm wt} = 500$ km is more consistent with a weak explosion, we focus on this case. Assuming that Sr and Zn made in the NDW are ejected with the same fraction, we obtain [Sr/Zn] = −1.4, −0.3, and 0.1 without flavor oscillations, with intermediate flavor conversion, and with complete flavor equilibration, respectively. Clearly, only with fast flavor oscillations is it possible to explain the observed [Sr/Zn] by the NDW. Note that while ^{64}Zn is the dominant Zn isotope, the contribution from other Sr isotopes is comparable to that from ^{84}Sr for complete flavor equilibration. To explain the observed [Zn/Fe] = 0.80 $\pm$ 0.25, we note that the Zn and Fe from the NDW would give [Zn/Fe] = 1.7–1.8 with fast flavor oscillations, which represents an upper limit had there been no Fe contributed from explosive nucleosynthesis. The observed [Zn/Fe], as well as [Sr/Fe] = [Sr/Zn] + [Zn/Fe], can be accounted for if the ejected Fe from explosive nucleosynthesis is $\sim$10 times more than that from the NDW.

Although looking for a CCSN model that matches the above constraints is beyond the scope of this study, we can use the observed value of [Fe/H] = −5.2 for HE 1327–2326 (Ezzeddine et al. 2019) to estimate the fraction of NDW material that needs to be included in the ejecta. To explain this [Fe/H], $\sim$10^{-5}–10$^{-4}\,M_\odot$ of Fe is needed to mix with $\sim$10^3–10$^4\,M_\odot$ of ISM. Because only $\sim$10% of this Fe is from the NDW but $\sim$10$^{-3}\,M_\odot$ of Fe is produced there, we estimate that $\sim$(0.1–1)% of the NDW material is mixed into the ejecta. We consider that the above scenario of a low-metallicity CCSN
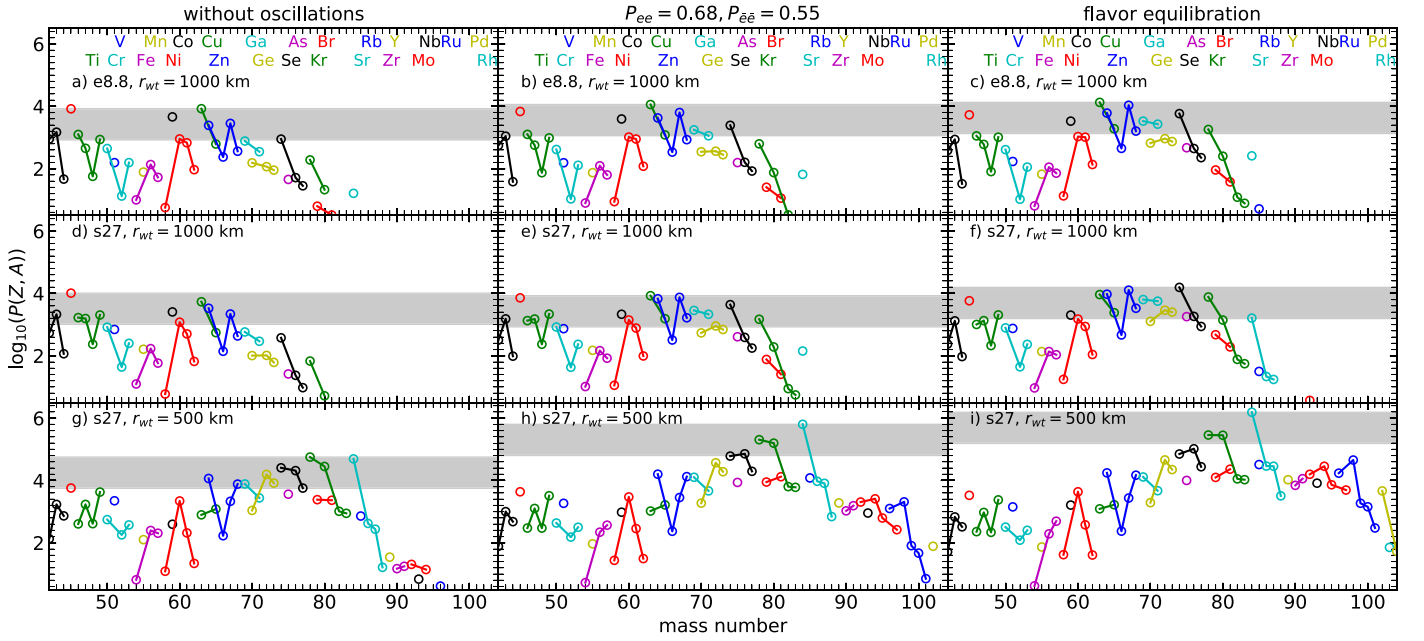
Figure 7. Production factors $P(Z, A)$ for all the NDW models. Isotopes of the same element are connected by line segments. Nuclei in the gray bands have production factors exceeding 0.1 times the corresponding maximum value.

with mixing and fallback, including the NDW contributions with fast flavor oscillations, may explain the high values of both [Zn/Fe] and [Sr/Fe] for HE 1327–2326. We refer readers to Heger & Woosley (2010) and Ezzeddine et al. (2019) for detailed discussions of CCSN models that may fit the overall abundance pattern of this star.

5.2. Galactic Chemical Evolution

We expect that the yields from our NDW models apply generally to NDWs in CCSNe, with progenitors and neutrino emission similar to those considered here. Under this expectation, we can estimate the dominant contributions from such NDWs to the present Galactic inventory of nuclei. Taking the solar composition (Asplund et al. 2009) as representative of this inventory, we can identify the significant nuclei contributed from a NDW model by considering the production factor $P(Z, A) = X(Z, A)/X_\odot(Z, A)$, where $X(Z, A)$ is the mass fraction of the nucleus with charge number Z and mass number A produced in the model. Figure 7 shows $P(Z, A)$ for all our models. Nuclei within the gray bands have production factors exceeding 0.1 times the maximum value P_{max}, and therefore their production by NDWs can potentially make significant to dominant contributions to their present Galactic inventory. The actual NDW contributions, however, also depend on the net mass loss and the frequency of occurrences for the relevant source.

We first discuss the nuclei in the gray bands in Figure 7. For model e8.8 without flavor oscillations, $P_{max} = 8.4 \times 10^3$ corresponds to ^{63}Cu, a result of proton-rich freeze-out from NSE (e.g., Fröhlich et al. 2006a). Other nuclei in the band include ^{67}Zn, ^{64}Zn, and the light p-nucleus ^{74}Se. With fast flavor oscillations, P_{max} still corresponds to ^{63}Cu, but its value is increased by a factor of 1.4–1.6. The production factors of ^{67}Zn, ^{64}Zn, and ^{74}Se are increased by a factor of 2.2–3.8, 1.7–2.5, and 2.8–6.6, respectively. In addition, the light p-nucleus ^{78}Kr is added to the gray band for complete flavor equilibrium. The general effects of fast flavor oscillations to increase production

factors and extend the range of significant production to heavier nuclei also apply to model s27. For $r_{wt} = 1000$ km, $P_{max} = 1.0 \times 10^4$, 8.4×10^3, and 1.6×10^4 corresponds to ^{45}Sc without flavor oscillations, ^{63}Cu with intermediate flavor conversion, and ^{74}Se with complete flavor equilibrium, respectively. The nuclei ^{67}Zn, ^{64}Zn, and ^{74}Se have production factors of $\sim(0.5–1)P_{max}$ with fast flavor oscillations. In addition, ^{78}Kr is added to the gray band for intermediate flavor conversion, and another light p-nucleus, ^{84}Sr, is added for complete flavor equilibrium. For $r_{wt} = 500$ km, ^{78}Kr and ^{84}Sr have the largest production factors with or without flavor oscillations. Specifically, $P(^{78}$Kr$) = 5.6 \times 10^4$, 2.0×10^5, and 2.9×10^5 [$P(^{84}$Sr$) = 4.9 \times 10^4$, 6.3×10^5, and 1.5×10^6] without flavor oscillations, with intermediate flavor conversion, and with complete flavor equilibrium, respectively.

Assuming that each NDW model represents a CCSN source occurring in a total mass $M_{ISM} \sim 10^{11} M_\odot$ of ISM with an average frequency f_{NDW} over the Galactic history of duration $t_G \sim 10^{10}$ yr, we can estimate the fraction $f(Z, A)$ contributed by this source to the Galactic inventory of a nucleus with charge number Z and mass number A:

$$f(Z, A) = \frac{X(Z, A)M_{NDW}f_{NDW}t_G}{X_\odot(Z, A)M_{ISM}}$$

$$\sim \frac{P(Z, A)}{3 \times 10^5}\left(\frac{M_{NDW}}{10^{-3} M_\odot}\right)\left[\frac{f_{NDW}}{(30 \text{ yr})^{-1}}\right], \quad (12)$$

where M_{NDW} is the net mass loss of the NDW (see Table 1). For reasonable values of $f_{NDW} \lesssim (30 \text{ yr})^{-1}$, model e8.8 could contribute at most $\sim2\%$, $\sim4\%$, and $\sim6\%$ of the Galactic inventory of ^{63}Cu without flavor oscillations, with intermediate flavor conversion, and with complete flavor equilibrium, respectively. Because ^{63}Cu has the largest production factor, we conclude that these NDWs cannot make major contributions to the Galactic inventory of any nucleus. Model s27 with $r_{wt} = 1000$ km could make more significant contributions to

the Galactic inventory of the dominant products: up to $\sim$12% for ^{45}Sc without flavor oscillations, $\sim$12% for ^{63}Cu with intermediate flavor conversion, and $\sim$28% for ^{74}Se with complete flavor equilibration. Nevertheless, no major contributions to any nucleus are expected from these NDWs, either.

Model s27 with $r_{wt} = 500$ km is the most interesting. Without flavor oscillations, it could contribute up to $\sim$68% of the ^{78}Kr and $\sim$60% of the ^{84}Sr in the Galactic inventory. Because the production factors are increased significantly by fast flavor oscillations, we must limit the frequency of occurrences of the corresponding NDWs to avoid overproducing any nucleus, especially the dominant product ^{84}Sr. Specifically, for the model under discussion, NDWs with intermediate flavor conversion (complete flavor equilibration) could occur only with an average frequency of $\lesssim(280 \text{ yr})^{-1}$ [$\lesssim(850 \text{ yr})^{-1}$], corresponding to $\lesssim$11% ($\lesssim$3.5%) of the CCSNe.

The γ process can also produce p-nuclei during the evolution of a massive star and the explosive burning of CCSN ejecta. The yield of ^{84}Sr by this process varies greatly from $\sim$10^{-9} to $\sim$10^{-6} $M_\odot$ (e.g., Pignatari et al. 2016). For model s27 with $r_{wt} = 1000$ km, the ^{84}Sr yield from NDWs reaches the lower end of this range only with complete flavor equilibration (see Table 2). For model s27 with $r_{wt} = 500$ km, however, the ^{84}Sr yield from NDWs is already significant even without flavor oscillations and reaches the higher end of the above range with fast flavor oscillations. As we have shown above, if such NDWs with fast flavor oscillations were to occur in a relatively small fraction of CCSNe, they could dominate the Galactic inventory of ^{84}Sr. Of course, more studies are needed to quantify the actual contributions from these NDWs and the γ process.

5.3. Isotopic Anomalies in Meteorites

The widely varying production factors for each NDW model shown in Figure 7 mean that the production patterns for these NDWs differ greatly from the solar pattern. Consider CCSNe occurring at times close to the formation of the solar system. If some of the associated NDW material could condense into grains that would be incorporated into meteorites, then isotopic anomalies characteristic of NDW nucleosynthesis would be found in such meteorites. Specifically, there would likely be excesses of those nuclei in the gray bands shown in Figure 7. Note that even when a NDW source is not a major contributor to the Galactic inventory, it still can produce isotopic anomalies in meteorites so long as the relevant grains could be formed and incorporated into meteorites.

An excess of ^{84}Sr was found in Ca-Al-rich inclusions (CAIs) in the Allende meteorite (e.g., Brennecka et al. 2013; Burkhardt et al. 2019). As shown in Figure 7, this nucleus is the dominant product of NDWs for model s27 with $r_{wt} = 500$ km and with fast flavor oscillations while its isotopes are greatly suppressed. Therefore, such NDWs could be the source producing the observed excess of ^{84}Sr. Interestingly, excesses of ^{92,94,95,97,100}Mo were also found in the same Allende CAIs (Brennecka et al. 2013). Although our NDW models cannot account for such excesses, we note that neutron-rich NDWs, possibly from NSMs, could be a source for these Mo anomalies (Bliss et al. 2018).

6. Discussion and Conclusions

Using the unoscillated neutrino emission characteristics from two CCSN simulations (models e8.8 and s27) representative of relevant progenitors at the lower and higher mass end, we have studied the potential effects of fast flavor oscillations on NDWs and their nucleosynthesis. We find that such oscillations can increase the total mass loss by factors up to $\sim$1.5–1.7 and lead to significantly more proton-rich conditions. The latter effect can greatly enhance the production of ^{64}Zn and the so-called light p-nuclei ^{74}Se, ^{78}Kr, and ^{84}Sr.

Were fast flavor oscillations to occur close to the PNS surface as described here, they would have important implications for abundances in metal-poor stars, Galactic chemical evolution in general, and isotopic anomalies in meteorites (see Section 5). When such oscillations are included, the Zn from NDWs in model e8.8 could readily explain some of the data on [Zn/Fe] for metal-poor stars (Cayrel et al. 2004). In addition, the Zn and Sr from NDWs in model s27 with $r_{wt} = 500$ km could explain the high values of both [Zn/Fe] and [Sr/Fe] for HE 1327–2326 (Ezzeddine et al. 2019) in the context of mixing and fallback for a low-metallicity CCSN. While NDWs in models e8.8 and s27 with $r_{wt} = 1000$ km do not make major contributions to the present Galactic inventory even with fast flavor oscillations, their clearly nonsolar production patterns might result in isotopic anomalies if some NDW material could condense into grains that would be incorporated into meteorites. The observed excess of ^{84}Sr in the Allende CAIs (e.g., Brennecka et al. 2013; Burkhardt et al. 2019) might be explained by a source like the NDWs in model s27 with $r_{wt} = 500$ km and with fast flavor oscillations. The dominant production of ^{84}Sr by such a source, however, leads to a constraint that it can represent only $\lesssim$(3.5–11)% of CCSNe to avoid overproducing this nucleus.

Roberts et al. (2010) performed a hydrodynamic study of NDWs based on neutrino emission from CCSN simulations, including our model e8.8. Allowing for the effects of fast flavor oscillations not included in their study, their results are qualitatively similar to ours. There were also many parametric studies of NDW nucleosynthesis (e.g., Wanajo et al. 2011a; Bliss et al. 2018; Nishimura et al. 2019). The parameterization can be tuned to provide more extreme values of the entropy, Y_e, and hence, Δ_n, than what we find in our NDW models. When similar conditions are considered, our results are consistent with those of e.g., Wanajo et al. (2011a).
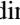
Using 1D and 2D simulations, Wanajo et al. (2009, 2011b) studied the nucleosynthesis in the early material ejected directly by the explosion of our e8.8 progenitor model. In addition, Wanajo et al. (2018) studied the nucleosynthesis for the 2D explosions of a number of progenitors, including those of 8.8 $M_\odot$ and 27 $M_\odot$. In contrast to the NDW, the CCSN simulations found a neutron-rich component of the early ejecta with Y_e down to $\sim$0.4, which also produces ^{64}Zn. For the 8.8 $M_\odot$ progenitor, Wanajo et al. (2009, 2011b) obtained $\sim$(6–7) × 10^{-6} $M_\odot$ of ^{64}Zn, comparable to our yields from the NDW. This neutron-rich component also produces mostly the neutron-rich isotopes of the elements up to Zr. For the proton-rich component of the early ejecta in the CCSN simulations, the Y_e can be up to $\sim$0.56 and $\sim$0.6 for the 8.8 $M_\odot$ and 27 $M_\odot$ progenitors, respectively. In these conditions, Wanajo et al. (2018) also found a weak νp process producing the light p-nuclei ^{74}Se, ^{78}Kr, and ^{84}Sr. For these nuclei, they obtained yields that are $\sim$10–1000 times larger than those for our NDWs

in the case of the 8.8 $M_\odot$ progenitor. For the 27 $M_\odot$ progenitor, however, they obtained comparable yields to those for our NDWs with $r_{wt} = 500$ km. Recent 3D simulations by Burrows et al. (2020) also confirmed the predominant proton-richness of the inner ejecta and reported a wind-like component. Considering the similarity of the conditions between the early proton-rich ejecta and the NDWs, we expect that the potential effects of fast flavor oscillations on the nucleosynthesis for the former are qualitatively similar to those found here for the latter. The early neutron-rich ejecta (e.g., Wanajo et al. 2009, 2011b; Eichler et al. 2018), however, require a separate study.

Although we have explored the potential effects of fast flavor oscillations on NDWs and their nucleosynthesis, two important questions remain to be investigated for various CCSN simulations: can such oscillations occur close to the PNS surface, and if so, with what flavor conversion efficiency? Further efforts to address the above questions are crucial to support the important implications of fast flavor oscillations for abundances in metal-poor stars, Galactic chemical evolution in general, and isotopic anomalies in meteorites as discussed here.

ORCID iDs

Zewei Xiong https://orcid.org/0000-0002-2385-6771
Andre Sieverding https://orcid.org/0000-0001-8235-5910
Manibrata Sen https://orcid.org/0000-0001-7948-4332
Yong-Zhong Qian https://orcid.org/0000-0002-3146-2668

References

Abbar, S., & Duan, H. 2018, PhRvD, 98, 043014
Abbar, S., Duan, H., Sumiyoshi, K., Takiwaki, T., & Volpe, M. C. 2020, PhRvD, 101, 043016
Abbar, S., & Volpe, M. C. 2019, PhLB, 790, 545
Arcones, A., & Janka, H. T. 2011, A&A, 526, A160
Arcones, A., Janka, H. T., & Scheck, L. 2007, A&A, 467, 1227
Arcones, A., & Thielemann, F. K. 2013, JPhG, 40, 013201
Asplund, M., Grevesse, N., Sauval, A. J., & Scott, P. 2009, ARA&A, 47, 481
Audi, G., Kondev, F. G., Wang, M., Huang, W. J., & Naimi, S. 2017, ChPhC, C41, 030001
Bethe, H. A. 1990, RvMP, 62, 801
Bliss, J., Arcones, A., & Qian, Y. Z. 2018, ApJ, 866, 105
Brennecka, G. A., Borg, L. E., & Wadhwa, M. 2013, PNAS, 110, 17241
Burkhardt, C., Dauphas, N., Hans, U., Bourdon, B., & Kleine, T. 2019, GeoCoA, 261, 145
Burrows, A., Radice, D., Vartanyan, D., et al. 2020, MNRAS, 491, 2715
Capozzi, F., Dasgupta, B., Lisi, E., Marrone, A., & Mirizzi, A. 2017, PhRvD, 96, 043016
Capozzi, F., Dasgupta, B., Mirizzi, A., Sen, M., & Sigl, G. 2019, PhRvL, 122, 091101
Cayrel, R., Depagne, E., Spite, M., et al. 2004, A&A, 416, 1117
Cyburt, R. H., Amthor, A. M., Ferguson, R., et al. 2010, ApJS, 189, 240
Dasgupta, B., Mirizzi, A., & Sen, M. 2017, JCAP, 1702, 019
Dasgupta, B., & Sen, M. 2018, PhRvD, 97, 023017
Delfan Azari, M., Yamada, S., Morinaga, T., et al. 2019, PhRvD, 99, 103011
Delfan Azari, M., Yamada, S., Morinaga, T., et al. 2020, PhRvD, 101, 023018
Duan, H., Fuller, G. M., & Qian, Y.-Z. 2010, ARNPS, 60, 569
Eichler, M., Nakamura, K., Takiwaki, T., et al. 2018, JPhG, 45, 014001
Ezzeddine, R., Frebel, A., Roederer, I. U., et al. 2019, ApJ, 876, 97
Fischer, T., Martínez-Pinedo, G., Hempel, M., & Liebendörfer, M. 2012, PhRvD, 85, 083003
Frebel, A. 2018, ARNPS, 68, 237
Fröhlich, C., Hauser, P., Liebendörfer, M., et al. 2006a, ApJ, 637, 415
Fröhlich, C., Martínez-Pinedo, G., Liebendörfer, M., et al. 2006b, PhRvL, 96, 142502
Fuller, G. M., Mayle, R., Meyer, B. S., & Wilson, J. R. 1992, ApJ, 389, 517
Glas, R., Janka, H.-T., Capozzi, F., et al. 2020, PhRvD, 101, 063001
Heger, A., & Woosley, S. E. 2010, ApJ, 724, 341
Hoffman, R. D., Woosley, S. E., Fuller, G. M., & Meyer, B. S. 1996, ApJ, 460, 478
Hüdepohl, L., Müller, B., Janka, H. T., Marek, A., & Raffelt, G. G. 2010, PhRvL, 104, 251101
Izaguirre, I., Raffelt, G. G., & Tamborra, I. 2017, PhRvL, 118, 021101
Janka, H.-T., Hanke, F., Hüdepohl, L., et al. 2012, PTEP, 2012, 01A309
Just, O., Bauswein, A., Ardevol Pulpillo, R., Goriely, S., & Janka, H. T. 2015, MNRAS, 448, 541
Martin, J. D., Yi, C., & Duan, H. 2019, PhLB, 800, 135088
Martínez-Pinedo, G., Fischer, T., & Huther, L. 2014, JPhG, 41, 044008
Mirizzi, A., Tamborra, I., Janka, H.-T., et al. 2016, NCimR, 39, 1
Möller, P., Pfeiffer, B., & Kratz, K.-L. 2003, PhRvC, 67, 055802
Nagakura, H., Morinaga, T., Kato, C., & Yamada, S. 2019, ApJ, 886, 139
Ning, H., Qian, Y. Z., & Meyer, B. S. 2007, ApJL, 667, L159
Nishimura, N., Rauscher, T., Hirschi, R., et al. 2019, MNRAS, 489, 1379
Nomoto, K. 1984, ApJ, 277, 791
Perego, A., Rosswog, S., Cabezón, R. M., et al. 2014, MNRAS, 443, 3134
Pignatari, M., Herwig, F., Hirschi, R., et al. 2016, ApJS, 225, 24
Pruet, J., Hoffman, R. D., Woosley, S. E., Janka, H. T., & Buras, R. 2006, ApJ, 644, 1028
Pruet, J., Woosley, S. E., Buras, R., Janka, H. T., & Hoffman, R. D. 2005, ApJ, 623, 325
Qian, Y.-Z., Fuller, G. M., Mathews, G. J., et al. 1993, PhRvL, 71, 1965
Qian, Y. Z., & Woosley, S. E. 1996, ApJ, 471, 331
Richers, S. A., McLaughlin, G. C., Kneller, J. P., & Vlasenko, A. 2019, PhRvD, 99, 123014
Roberts, L. F., Woosley, S. E., & Hoffman, R. D. 2010, ApJ, 722, 954
Sawyer, R. F. 2009, PhRvD, 79, 105003
Sieverding, A., Martínez-Pinedo, G., Huther, L., Langanke, K., & Heger, A. 2018, ApJ, 865, 143
Tanabashi, M., Hagiwara, K., Hikasa, K., et al. 2018, PhRvD, 98, 030001
Travaglio, C., Rauscher, T., Heger, A., Pignatari, M., & West, C. 2018, ApJ, 854, 18
Wanajo, S., Janka, H.-T., & Kubono, S. 2011a, ApJ, 729, 46
Wanajo, S., Janka, H.-T., & Müller, B. 2011b, ApJL, 726, L15
Wanajo, S., Müller, B., Janka, H.-T., & Heger, A. 2018, ApJ, 852, 40
Wanajo, S., Nomoto, K., Janka, H. T., Kitaura, F. S., & Müller, B. 2009, ApJ, 695, 208
Wilson, J. R., & Mayle, R. W. 1993, PhR, 227, 97
Woosley, S. E., Heger, A., & Weaver, T. A. 2002, RvMP, 74, 1015
Wu, M.-R., & Tamborra, I. 2017, PhRvD, 95, 103007
Wu, M.-R., Tamborra, I., Just, O., & Janka, H.-T. 2017, PhRvD, 96, 123015
Xiong, Z., Wu, M.-R., & Qian, Y.-Z. 2019, ApJ, 880, 81
Yi, C., Ma, L., Martin, J. D., & Duan, H. 2019, PhRvD, 99, 063005